International Journal of GEOMATE, Oct., 2022, Vol.23, Issue 98, pp.66-74
ISSN: 2186-2982 (P), 2186-2990 (O), Japan, DOI: https://doi.org/10.21660/2022.98.3443
Geotechnique, Construction Materials and Environment

EXPERIMENTAL STUDY ON MICROSTRUCTURAL EVOLUTION AND DYNAMIC PROPERTIES OF A LOW-CARBON STEEL

*Ngoc-Vinh Nguyen[1], Nguyen Dinh Duc[2], Nguyen Vu-Luat[3], *Thai-Hoan Pham[4]

[1]Faculty of Advanced Technology and Engineering, VNU Vietnam Japan University, Vietnam
[2]Department of Engineering and Technology in Constructions and Transportation, VNU Hanoi, University of Engineering and Technology, Vietnam
[3]Dept. of Civil and Environmental Engineering, Mien Dong Innovative Technology University, Vietnam
[4]Faculty of Building and Industrial Construction, Hanoi University of Civil Engineering, Viet Nam

*Corresponding Author, Received: 04 May 2022, Revised: 24 Aug. 2022, Accepted: 09 Oct. 2022

ABSTRACT: In this study, dynamic tensile experiments were performed at a wide range of loading speeds from 1 mm/s to 1000 mm/s to investigate the microstructural evolution under high rates and ractccte-dependent behavior of mechanical properties of SM490 structural steel. The evolution of microstructure under different loading speeds or strain rate levels was observed. At a loading speed of 1 mm/s, partially broken original ferrite grains under the applied tensile loading resulted in the formation of smaller ferrite grains and packets of dislocation debris. The debris could be observed to be located inside original ferrite grains, while pearlite grains tended to move closer together, becoming the thin layers of pearlite. At the highest loading speed, pearlite thin layers were fully developed leading to the formation of the layers of ferrites. The averaged grain size tended to decrease with the further increase of loading speed. Both yield stress (σ_{y}) and tensile strength (σ_{u}) displayed rate-dependent behavior, in which higher σ_{y} could be observed at higher loading speed levels. In contrast, the work hardening (n) showed different behavior. n exhibited a slight increase when the loading speed increased from 1 mm/s to 10 mm/s, and then gradually decreased with the increasing speed of loading. Another plastic property (α) showed a decrease from 10.7 to 5.28 with increasing loading rate from 1 mm/s to 1000 mm/s. Finally, strain rate sensitivity values of 0.0428 from the σ_{y} data and 0.0226 from the σ_{u} data were well determined and reported for the tested material.

Keywords: Dynamic properties, Rate-dependent behavior, Strain rate sensitivity, Structural steel

1. INTRODUCTION

Structural steels are widely used materials in civil and industrial building construction as well as in other structural applications [1] owing to their advantageous features such as excellent machinability and weldability [2,3]. The usage of structural steel has several advantages compared to reinforced concrete (RC). For example, structural steel has a high strength per unit of weight [4], meaning that the weight of structures will be smaller than those of RC structures [5]. This fact is of great importance for tall buildings, long-span bridges, and structures situated on poor foundations. Furthermore, ductility has been attributed to another important aspect of structural steel, by which it can withstand extensive deformation without failure under high tensile stresses [6]. Since structural steel is very durable, the structures made by structural steel can withstand external pressures such as thunderstorms, cyclones, and earthquakes [7,8]. Therefore, much attention has been paid to the characterization of the affecting factors on the mechanical properties of structural steels as well as in their weld joints [9–13].

Pham and Kim [14] characterized the mechanical properties of microstructural phases and materials within the weld zone of SM520 structural steel using the depth-sensing instrument (DSI) technique. The indentation responses indicated that two different stiffness ferrite types were observed in each region of the weld zone from the analysis of elastic modulus (E) and hardness (H) results. Both H and σ_{y} of ferrite and pearlite phases increase from base metal (BM) to heat-affected zone (HAZ) due to the grain refinement and the change of grain morphology in the HAZ region during the welding process. Kim et al. [15] investigated the distribution of mechanical properties along the weld cross-section of SS400 structural steel weld joint using finite element (FE) analysis and the DSI technique. The variation of mechanical properties in three regions of the weld zone was discovered, in which BM has lower values of mechanical properties (E, H, σ_y and work hardening n) than those of the weld metal (WM). Mechanical properties within the HAZ region gradually increase from the BM to WM regions. The formation of the microstructure in the weld zone was also observed and the higher amount of δ-ferrite and its abundant transformed phase boundaries may be responsible for the higher mechanical property values in the WM when compared to those in the BM, while the smaller and more regular sizes of ferrite grains in the HAZ may be mainly responsible for the higher mechanical property values in the HAZ when compared to those in the BM. Kato et al. [16] standardized the mathematical expression for stress-strain relations of structural steel under monotonic and uniaxial tension loading, while the behavior and design of structural steel pins have been studied by Bridge et al. [17]. Kim et al. [18] studied the influences of the poly crystal boron nitride tool in friction stir weld steels, evaluated using the secondary ion mass spectroscopy technique. Recently, high-temperature strength and microstructural evolution in the weld coarse-grained HAZ of Fire-Resistant Steels was conducted by Moon et al. [19]. The study showed that the fire-resistance properties deteriorated in the HAZs compared to the BM steels since the yield stress of HAZ was demonstrated to be higher than those of BM steels at room and high temperatures [19].

The plastic flow behaviors and the corresponding deformation mechanisms are highly dependent on the loading rate (or strain rate) for both metals and alloys [8,20–22]. Khalifeh et al. [8] investigated the tensile mechanical properties of structural steels at a range of strain rate from 0.001 s^{-1} to 0.1 s^{-1}, and the influences of strain rate on several types of structural steels, for example, St37 and St53, were well characterized. Since the structures made from structural steel have a great ability to resist earthquakes due to their energy dissipation capacity and ductility, dynamic mechanical properties under high loading rates are very important for the structural integrity of steel structures [23]. Therefore, the dynamic behavior of structural steel needs to study more. In this study, the dynamic tensile loading experiments were used to investigate the evolution of microstructure under high loading speeds as well as the rate-dependent behavior of SM490 structural steel. For this purpose, dynamic tensile experiments were performed at a wide loading speed range from 1 mm/s to 1000 mm/s using the high-speed 250 kN actuator. Additionally, the evolution of microstructure under different loading rate conditions was also observed using an optical microscope examination. The dependences of E, σ_y, σ_u, n, and a plastic property α were also characterized.

2. RESEARCH SIGNIFICANCE

The significance of the study is to have a better understanding of the dynamic behavior of low-carbon steel at high strain rate levels. The microstructural evolution under high loading rates was observed and analyzed. In addition, dynamic properties of tested material as well as the strain rate sensitivity behavior was investigated giving the significant information in practical designs and engineering analysis.

3. EXPERIMENTAL PROCEDURES

The investigated material in this study is SM490 structural steel that has been attributed to rolled steel for welded structures, fabricated followed by a Japanese standard (JIS G 3106) [24]. This structural steel has the chemical compositions as C0.16%, Si 0.4%, P0.01%, S0.003%, Mn1.45%, and Fe balanced [7]. The tensile specimens were cut out from the steel plates with a thickness of 12.5 mm for high strain rate tensile experiments. It can be seen in Fig. 1, these specimens have 50 mm length gauge and 12.5 mm thickness.

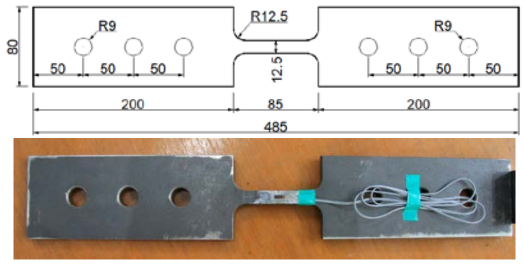

Fig. 1 Shape and dimension in *mm* of sample for high-speed tensile experiments

Three high-strength bolts were employed to grip the specimen for both upper and lower grips to reduce the influences of high loading speed. 250 kN actuator was selected to perform all tensile experiments in this study and a servo-hydraulic system was also used to generate a maximum actuator speed of 1000 mm/s, as illustrated in Fig. 2. The testing temperature was 296 K. The accuracy of the testing system was verified by comparing the yield stress obtained from the present testing system with those measured from the traditional tensile loading experiment, and the relative error of estimated yield stress must be less than 5%.

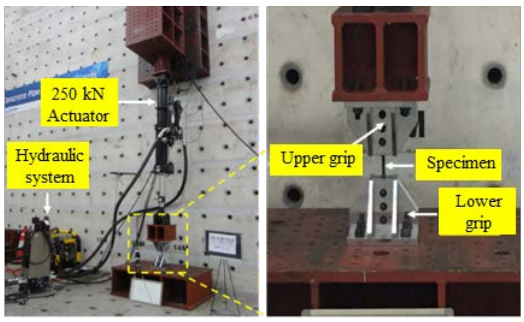

Fig. 2 Setup of dynamic tensile experiments

Dynamic tensile experiments were then carried out at several loading speeds, for example, 1 mm/s, 10 mm/s, 100 mm/s, 500 mm/s, and 1000 mm/s. To improve the accuracy of measurements at high loading rates, the strain gauge with a type of FLA-5-11-1L was employed and installed at the middle region of the length gauge. At least three tensile experiments were conducted for a loading speed level. To reveal the microstructure of the failure samples after high-speed tensile tests, the optical microscope (OM) examination was conducted. The OM specimens were cut out from the failure specimens (see Figs. 3a and 3b) and then put into the epoxy circle mold with a size of 25 mm diameter. These samples were then polished using several poly diamond papers to obtain the flat surface. It should be noted that the above procedure must ensure seven stages of increasing fineness, in which the last stage is 40 nm. To reveal the microstructure, the flat surfaces of these OM samples were etched using an acid solution of HNO_3 in 30 seconds.

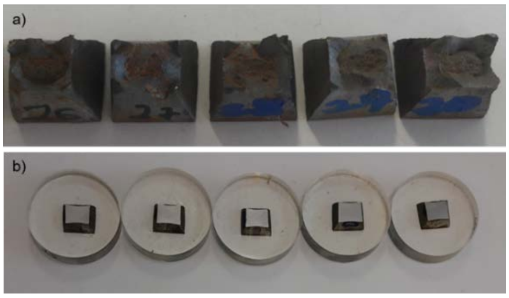

Fig. 3 Specimens for SEM examination: a) failure specimens form high-speed tensile tests, b) mounted and polished specimens for SEM

4. RESULTS AND DISCUSSION

4.1 Microstructure evolution under high loading rates

In this section, the evolution of microstructure under loading rate conditions was observed using the optical microscope examination. The microstructure of the virgin specimen has been presented elsewhere [25]; however, an observation was still conducted for comparison purposes.

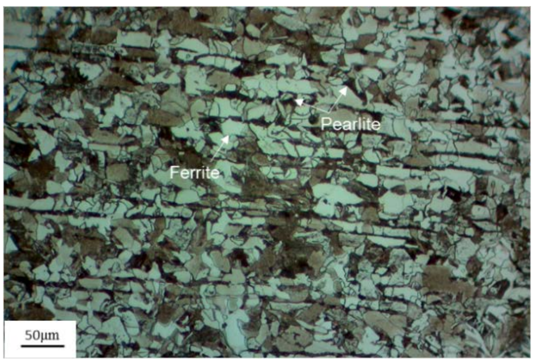

Fig. 4 Microstructure of the virgin specimen including ferrite/pearlite structures

It can be seen from Fig. 4 that SM490 structural steel is composed of ferrite and a small region of pearlite. Ferrite has many different shapes and sizes. To observe the variation of ferrite grain size, the histograms showing the statistic of grain size distribution were prepared as illustrated in Fig. 6a. The grain size of ferrite varies from 5.7 μm to 47.4 μm, in which the main grains have a size from 9.1 μm to 19.6 μm, leading to the average grain size of 16.12±8.15 μm. Occasionally, there are larger grains with an unusual size from 33.5 μm to 47.4 μm; however, they appear less frequently than smaller grains. In contrast, pearlites, dark-colored grains, are often located at the corner of ferrite grains or the grain boundary edges as seen in Fig. 4. The pearlite grains also have many types of shapes, such as the thin layer of pearlite, the rectangular pearlite, the circle pearlite, and so on.

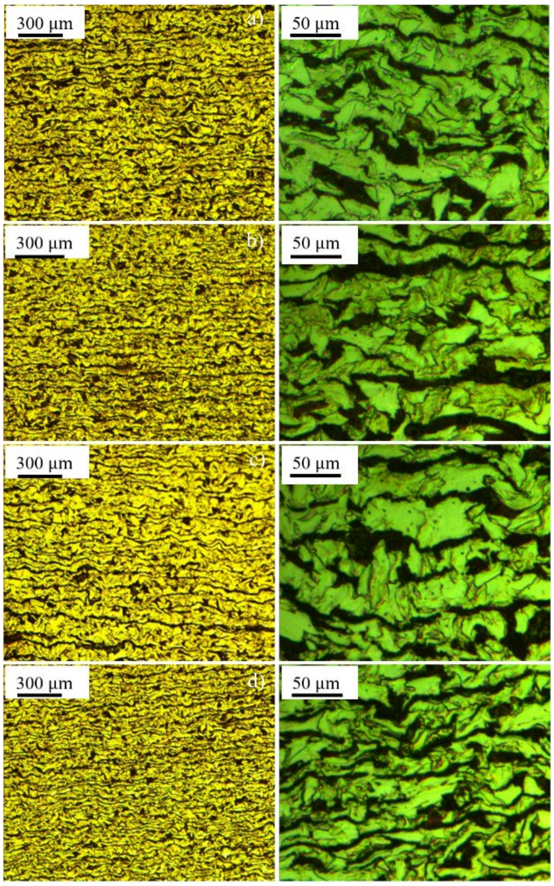

Fig. 5 Microstructure changes under high-speed conditions: a) microstructure at a strain rate of 0.02 s^{-1}, b) microstructure at a strain rate of 0.2 s^{-1}, c) microstructure at a strain rate of 1 s^{-1}, and d) microstructure at a strain rate of 20 s^{-1}

At a low loading rate of 1 mm/s, the original ferrite grains are partially broken, leading to the formation of smaller ferrite grains and the packets of dislocation debris as observed in Figs. 5a and 6b. The debris is mostly located inside original ferrite grains, while pearlite grains tend to move closer together, becoming the thin pearlite layers. These thin layers separate the ferrite grains and the packets of dislocation debris. The size of pearlite grain is observed to be relatively larger than those in the virgin sample. Under tensile loading, the ferrite grains tend to transform into the thin layers interspersed with the pearlite layers. The dislocation lines appear inside the ferrite grains. At a higher loading rate, the original grains are almost broken, and the debris is observed to appear more frequently. Due to the higher loading rate, the thin layers of pearlite were formed, leading to the smaller ferrite grains as seen in Fig. 6.

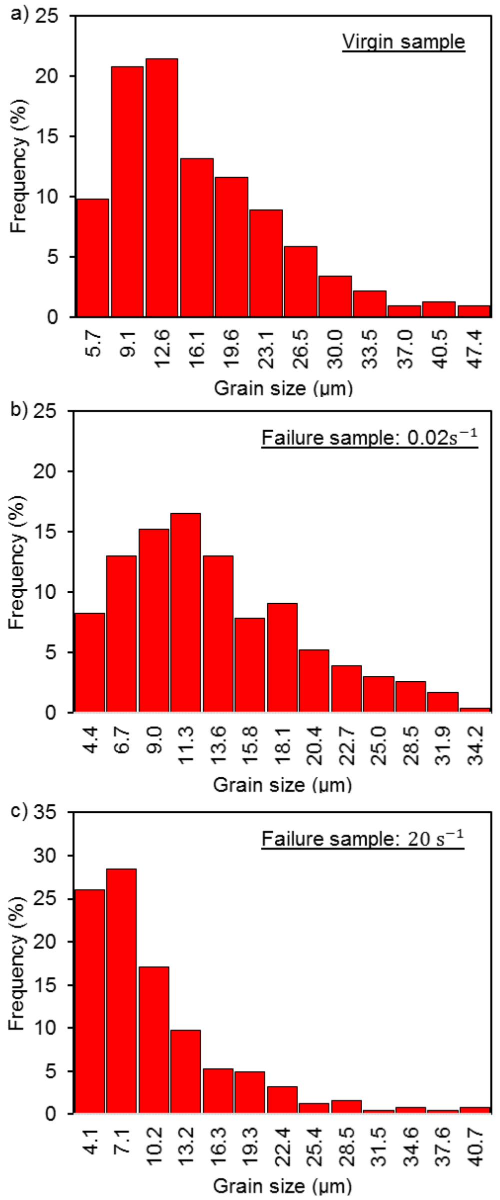

Fig. 6 Histograms showing the statistic of the grain size distribution: a) virgin sample, b) failure sample at 0.02 s^{-1}, and c) failure sample at 20 s^{-1}

The dislocation lines appear more frequently and are arranged within the interior grains. At the highest loading speed (1000 mm/s), the pearlite thin layers are fully developed leading to the formation of the layers of ferrites. The packets of dislocation debris are formed more frequently than the observation at other strain rate levels as illustrated in Fig. 5. It can be seen from the histograms of the grain size distributions in Fig. 6 that the size of major grains tends to decrease when the loading rate increase from 1 mm/s to 1000 mm/s. Indeed, it can be seen from Figs. 6a, 6b, and 6c that the mean value of grain size measured on the virgin sample (16.12±8.25 μm) is higher than those obtained for failure samples at the loading rate of 1 mm/s (13.75±7.23 μm) and the loading rate of 1000 mm/s (9.97±7.50 μm). That means the grain size at a lower loading rate level might be relatively higher than those at a higher loading rate.

4.2 Dynamic properties of SM490 structural steel

Nominal engineering stress-engineering strain curves of SM490 steel obtained from high-speed tensile experiments were shown in Fig. 7. As seen, the results of high-speed tensile experiments (i.e. at 100 mm/s, 500 mm/s, and 1000 mm/s) show the oscillation of load signal due to ringing of the loading system; however, the productivity parts are still good. The results exhibit that the loading speed influences not only on the shape but also on the magnitude of the engineering stress - strain curves. However, the elastic modulus seems to be independent of the strain rate level as seen in Fig. 7.

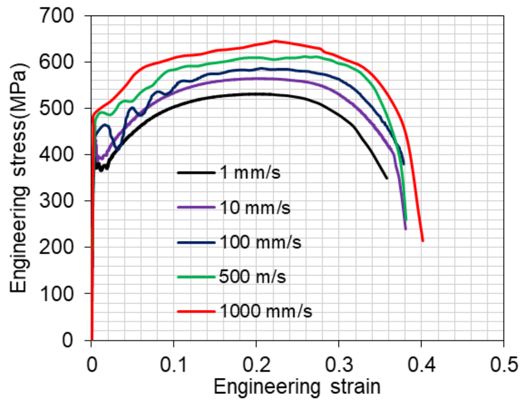

Fig. 7 Engineering stress-engineering strain curves at loading speeds

Indeed, the variation of E under a high loading rate is so slight and close to an averaged value of 211.03 GP, as shown in Fig. 8a, indicating that E seems to be independent of the variation of loading speed [26]. In contrast, the influences of loading rate on the plastic plateau are quite clear. As seen in Fig. 7, the presence of the plastic plateau stage at a low loading rate can be easily observed; however, it becomes less pronounced when the loading rate increases.

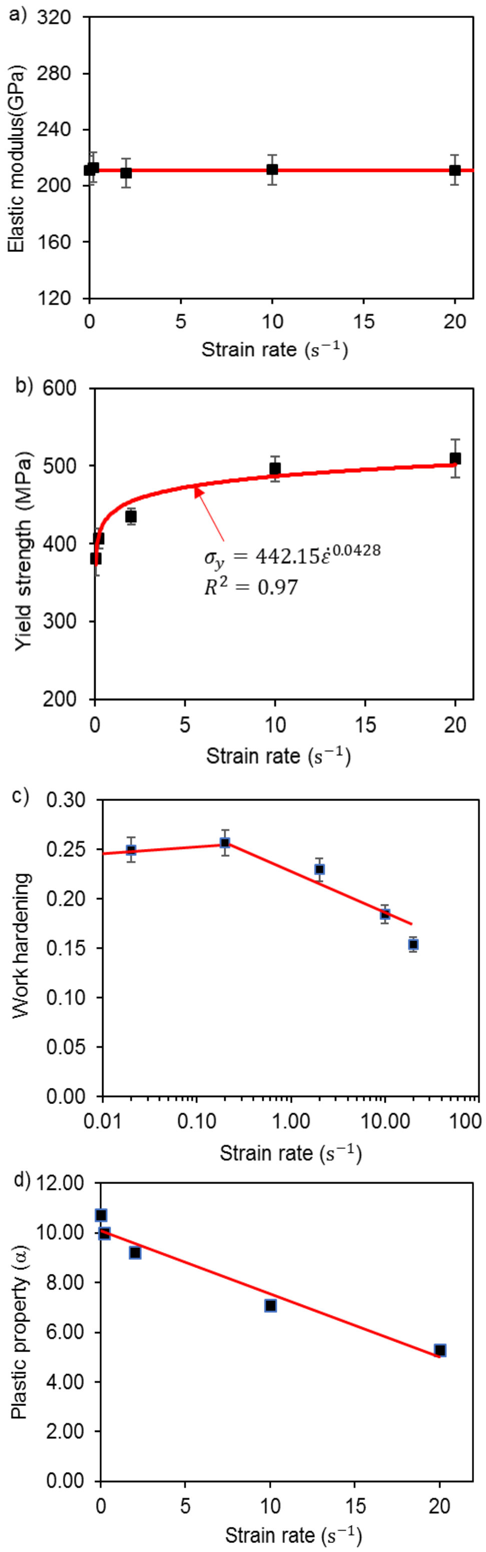

Fig. 8 Rate-dependent behavior of (a) elastic modulus, (b) yield stress, (c) work hardening, and (d) plastic properties α

Fig. 8b shows the rate-dependent behavior of σ_y. It should be noted that the σ_y values were calculated using the 0.2% offset method [27]. The σ_y tends to increase with the further increase of the loading speeds. Indeed, σ_y shows a rapid increase from 381.56 MPa to 496.15 MPa when lthe oading speed increases from 1 mm/s to 500 mm/s and slightly increases when the loading speed is greater than 500 mm/s. The rate-dependent behavior of n is quite different as illustrated in Fig. 8c. As seen, n increases with increasing loading rate from 1 mm/s to 100 mm/s and then decreases gradually when the loading rate is greater than 100 mm/s. The remaining plastic property(α) exhibits an inverse behavior compared to σ_y, in which α shows a gradual decrease from 10.70 to 5.28 with an increasing loading rate from 1 mm/s to 1000 mm/s. Another interesting feature from Fig. 8 is that a power-law function, $\sigma_y = 442.15\dot{\varepsilon}^{0.0428}$, can be used to predict the values of σ_y at a strain rate or a loading rate level. It is worth noting that strain rate ($\dot{\varepsilon}$) could be easily determined based on the loading rate (dL/dt) as $\dot{\varepsilon} = dL/L_0dt$, whereas L_0 is the original length. The results from the present study are totally consistent with the general trend reported in the literature [23,28–33].

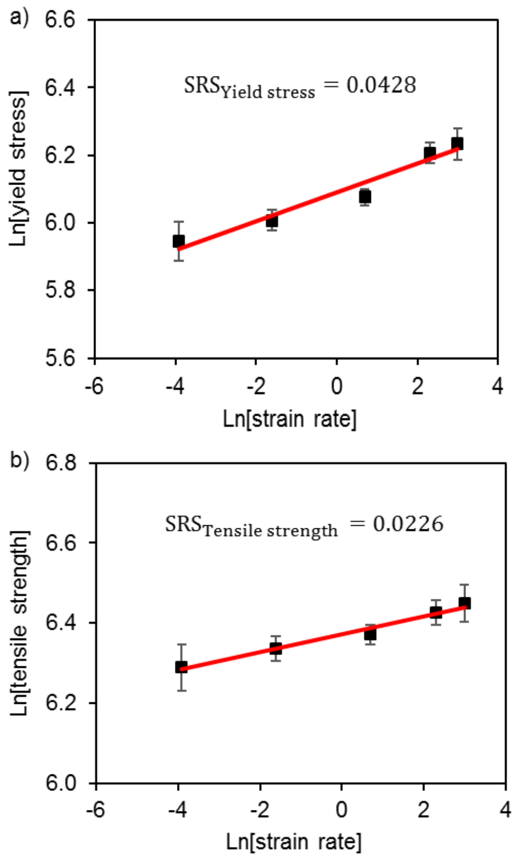

Fig. 9 Estimation of strain rate sensitivity of SM490 structural steel: a) yield stress data and b) tensile strength data

The results of σ_y and σ_u can be used to determine the values of strain rate sensitivity (SRS) using the following equation [23]:

$$\mathrm{SRS}_{\text{yield stress}} = \left(\frac{\partial \ln(\sigma_y)}{\partial \ln(\dot{\varepsilon})}\right)_T, \quad (1)$$

$$\mathrm{SRS}_{\text{tensile strength}} = \left(\frac{\partial \ln(\sigma_u)}{\partial \ln(\dot{\varepsilon})}\right)_T. \quad (2)$$

In Eqs. (1) and (2), a notation T is the temperature. Since all experiments in this study were performed at room temperature, mechanical properties depend only on the loading rate or strain rate. Regression analysis was then conducted to estimate SRS values for both σ_y and σ_u data as presented in Figs. 9a and 9b, respectively. As a result, the SRS value of 0.0428 from the σ_y data was well obtained, while the σ_u data provided an SRS value of 0.0226. The positive values of SRS for both σ_y and σ_u are caused by the following aspects. First, higher flow stress is measured at higher loading rate/higher strain rate levels since the higher strain rate may decelerate the dislocation annihilation [26]. Second, a higher loading rate or higher strain rate might increase the obstructions (or barriers) of the dislocation motions for the thermal and mechanically activated plastic deformation [34]. Indeed, as previously mentioned, the ferrite grains were forced to be broken when the applied loading speed increased (see Fig. 5), resulting in the formation of smaller ferrite grains and packets of dislocation debris. As shown in Fig. 5 and Fig. 6, the grain size was observed to decrease with the further increase of strain rate. Furthermore, Wellman [35] demonstrated that smaller grains have greater ratios of surface area to volume, which means a greater ratio of grain boundary to dislocations. That means the decrease of grain size absolutely increases the grain boundary as well as the barriers of the dislocation motion since the grain boundary is a major factor to impede the dislocation movements from grain to grain [36–38].

Another interesting feature in Figs. 9 and 10 is that the SRS value from the σ_y data is relatively higher than those calculated based on the σ_u data. Luecke et al. [23] performed the traditional tensile loading experiments on several types of steels to achieve the σ_y and σ_u data, which are necessary to determine the values of SRS. The results of their research indicated that the SRS values from the σ_y data are relatively higher than those calculated from the σ_u data. That means the present SRS values are in good agreement with the general trend reported in the literature [23,28,30–32,39]. By collecting the SRS data of many types of structural steels, both σ_y - SRS and σ_u - SRS relationships were constructed as shown in Fig. 10.

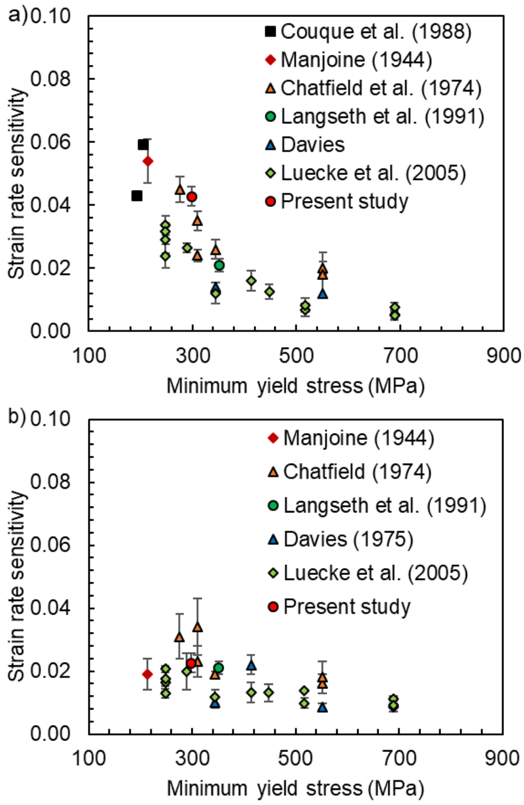

Fig. 10 Comparison of SRSs of the present study to values for several structural steels in the literature: a) yield stress data and b) tensile strength data

As seen in Fig. 10, the present SRS values from both σ_y and σ_u data are totally consistent with the general trend reported for several types of structural steels in the literature. Furthermore, the SRS from σ_y and σ_u data are attributed to be a function of a specified minimum yield stress [23]. The SRS values from the σ_y data show a progressive decrease with the further increase of specified minimum yield stress (see in Fig. 10a). It is quite different from the case of the SRSs from the σ_u data. The SRS results show a slight decrease when the specified minimum yield stress increases from 100 MPa to 800 MPa as observed in Fig. 10b. It should be noted that the specified minimum yield stress is defined as the values obtained at a quasi-static strain rate (0.0001 s^{-1}). Although the collected SRS values of several structural steels were measured from different types of experiments, for example, torsion, tension, and compression experiments; however, the main purpose of the comparisons in Figs. 10a and 10b are to compare the present SRS values with the general trend reported for structural steels in the literature. Thus, the comparisons in Fig. 10 are acceptable.

5. CONCLUSIONS

In this study, dynamic tensile experiments were performed using the high-speed 250 kN actuator for a wide range of loading speeds to characterize the SRS behavior of mechanical properties of SM490 structural steel. The experimental data and the FE analysis results support the following conclusions.

- The grain size tended to decrease when the loading rate increased from 1 mm/s to 1000 mm/s.
- Elastic modulus can be observed to be independent of the variation of loading rates.
- Both yield stress and tensile strength displayed the rate-dependent behavior, in which higher yield stress could be observed at higher loading rate levels.
- Work hardening exhibited a slight increase when the loading rate increased from 1 mm/s to 10 mm/s, and then gradually decreased with the further increase of loading rate level up to 1000 mm/s, while α showed almost decrease from 10.7 to 5.28 when the loading rate increased.
- SRS value of 0.0428 obtained from yield stress data and 0.0226 from tensile strength data were well reported for the investigated material.

6. ACKNOWLEDGEMENT

This research is supported by a grant (CT.2019.03.05) from the Science and Technology program funded by the Ministry of Education and Training of Vietnam.

7. REFERENCES

[1] AbdElrahman A.M., Hussein M.M., Attia W.A.L. , Modified Web Slenderness Classification for Composite Girders in Code Provisions, International Journal of GEOMATE, Vol. 20, Issue 80, 2021, pp. 168–75.
DOI: 10.21660/2021.80.j2068.

[2] Tamboli A.R., Handbook of structural steel connections: design and details. Third edition, Mc Graw Hill Education, New York, United States, 1976, pp. 1-570.
ISBN: 9780070614970

[3] Banerjee K., Role of Base Metal Microstructure on Tensile Properties and Weldability of Simulated Continuously Annealed Advanced High Strength Steels, International Journal of Metallurgical Engineering, Vol. 2, Issue 1, 2013, pp. 100–110.
DOI: 10.5923/j.ijmee.20130201.15.

[4] De Jesus J.M.L., Lejano B.A., An investigation on the strength of axially loaded cold-formed steel Z-sections, International Journal of GEOMATE, Vol. 14, Issue 42, 2018, pp. 30–36.
DOI: 10.21660/2018.42.714.

[5] Jack C., McCormac, Stephen F. Csernak, Structural Steel Design. Fifth Edition, Prentice Hall, Inc., New York, United States, New York, 2012, pp. 1-738.
ISBN: 9780136079484

[6] Nguyen N.V., Pham T.H., Kim S.E., Characterization of strain rate effects on the plastic properties of structural steel using nanoindentation, Construction and Building Materials, Vol. 163, 2018, pp. 305–314.
DOI: 10.1016/j.conbuildmat.2017.12.122.

[7] Nguyen N.V., Pham T.H., Kim S.E., Strain rate sensitivity behavior of a structural steel during low-cycle fatigue investigated using indentation, Materials Science and Engineering A, Vol. 744, 2019, pp. 490–499.
DOI: 10.1016/j.msea.2018.12.025.

[8] Khalifeh A.R., Banaraki A.D., Manesh H.D., Banaraki M.D., Investigating of the tensile mechanical properties of structural steels at high strain rates, Materials Science and Engineering A, Vol. 712, 2018, pp. 232–241.

[9] Chung K.H., Lee W., Kim J.H., Kim C., Park S.H., Kwon D., et al., Characterization of mechanical properties by indentation tests and FE analysis - validation by application to a weld zone of DP590 steel, International Journal of Solids and Structures, Vol. 46, Issue 2, 2009, pp. 344–363.
DOI: 10.1016/j.ijsolstr.2008.08.041.

[10] Eroglu M., Aksoy M., Orhan N., Effect of coarse initial grain size on microstructure and mechanical properties of weld metal and HAZ of a low carbon steel, Materials Science and Engineering A, Vol. 269, 1999, pp. 59–66.
DOI: 10.1016/s0921-5093(99)00137-9.

[11] Kou S., Welding Metallurgy. Second edition, John Wiley & Sons, Inc. Hoboken, New Jersey, United States, 2003, pp.1-461, ISBN:9780471434023 `
DOI:10.1002/0471434027.

[12] Hoan P.T., Vinh N.N., Tung N.T.T., Indentation for investigation of strain rate effect on mechanical properties in structural steel weld zone, Journal of Science and Technology in Civil Engineering (STCE) - NUCE, Vol. 13, No. 3, 2019, pp. 104–112.
DOI: 10.31814/stce.nuce2019-13(3)-10.

[13] Pham T.H., Nguyen N.V., Mechanical properties of constituent phases in structural steels and heat-affected zones investigated by statistical nanoindentation analysis,

Construction and Building Materials, Vol. 268, 2021, pp. 121211.
DOI: 10.1016/j.conbuildmat.2020.121211.

[14] Pham T.H., Kim S.E., Characteristics of microstructural phases relevant to the mechanical properties in structural steel weld zone studied by using indentation, Construction and Building Materials, Vol. 155, 2017, pp. 176–186.
DOI: 10.1016/j.conbuildmat.2017.08.033.

[15] Kim J.J., Pham T.H., Kim S.E., Instrumented indentation testing and FE analysis for investigation of mechanical properties in structural steel weld zone, International Journal of Mechanical Sciences, Vol. 103, 2015, pp. 265–274.
DOI: 10.1016/j.ijmecsci.2015.09.015.

[16] Kato B., Aoki H., Yamanouchi H., Standardized mathematical expression for stress-strain relations of structural steel under monotonic and uniaxial tension loading, Materials and Structures, Vol. 23, 1990, pp. 47–58.
DOI: 10.1007/BF02472997.

[17] Bridge R.Q., Sukkar T., Hayward I.G., Van Ommen M., Behaviour and design of structural steel pins, Steel and Composite Structures, Vol. 1, 2001, pp. 97–110.
DOI: 10.12989/scs.2001.1.1.097.

[18] Kim J.N., Lee S.U., Kwun H.D., Shin K.S., Kang C.Y., SIMS evaluation of poly crystal boron nitride tool effect in the thermo-mechanically affected zone of friction stir weld steels, Metals and Materials International, Vol. 20, 2014, pp. 1067–1071.
DOI: 10.1007/s12540-014-6010-x.

[19] Moon J., Lee C.H., Jo H.H., Kim S.D., Hong H.U., Chung J.H., et al., Microstructure and High-Temperature Strength in the Weld Coarse-Grained Heat-Affected Zone of Fire-Resistant Steels and the Effects of Mo and Nb Additions, Metals and Materials International, Vol. 28, 2021, pp. 966-974.

[20] Yu H., Guo Y., Lai X., Rate-dependent behavior and constitutive model of DP600 steel at strain rate from 10-4 to 103 s-1, Materials and Design, Vol. 30, Issue 7, 2009, pp. 2501–2505.
DOI: 10.1016/j.matdes.2008.10.001.

[21] Singh N.K., Cadoni E., Singha M.K., Gupta N.K., Dynamic tensile behavior of multi-phase high yield strength steel, Materials and Design, Vol. 32, Issue 10, 2011, pp. 5091–5098.
DOI: 10.1016/j.matdes.2011.06.027.

[22] Yuan .F, Bian X., Jiang P., Yang M., Wu X., Dynamic shear response and evolution mechanisms of adiabatic shear band in the ultrafine-grained austenite-ferrite duplex steel, Mechanics of Materials, Vol. 89, 2015, pp. 47–58.
DOI: 10.1016/j.mechmat.2015.06.004.

[23] Luecke W.E. et al., Mechanical properties of structural steels, National Institute of Standards and Technology, Washington, United States, 2005, pp. 1-288.

[24] JIS G 3106. Rolled steels for welded structure, Japanese Industrial Standard, Vol. G 3106, 2004, pp. 1–33.

[25] Nguyen N.V., Pham T.H., Kim S.E., Microstructure and strain rate sensitivity behavior of SM490 structural steel weld zone investigated using indentation, Construction, and Building Materials, Vol. 206, 2019, pp. 410–418.
DOI: 10.1016/j.conbuildmat.2019.02.013.

[26] Wang W., Ma Y., Yang M., Jiang P., Yuan F., Wu X., Strain Rate Effect on Tensile Behavior for a High Specific Strength Steel : From Quasi-Static to Intermediate Strain Rates, Metals (Basel), Vol. 8, Issue 1, 2018, pp. 1–14.
DOI: 10.3390/met8010011.

[27] Subramanian K.N., Lead-Free electronic solders: Material in electronics, Springer, New York, United States, 2006, pp. 1-361.
ISBN: 9780387484334

[28] Nagaraja Rao N.R., Lohrmann M., Tall L., Effect of strain rate on the yield stress of structural steels, ASTM Journal of Materials, Vol. 1, No. 1, 1966, pp. 241–262.

[29] Kasada R., Ishii D., Ando M., Tanigawa H., Ohata M., Konishi S., Dynamic tensile properties of reduced-activation ferritic steel F82H, Fusion Engineering and Design, Vol. 100, Issue, 2015, pp. 146–151.

[30] Chatfield D.A., Rote R.R., Strain rate effects on properties of high strength, low alloys steels, Society Automotive Engineering, 1974, pp. 1–12.

[31] Manjoine M.J., Influence of rate of strain and temperature on yield stresses of mild steel, Journal of Applied Mechanics, Vol. 11, Issue 4, 1944, pp. 211–218.

[32] Davies R.G., Magee C.L., The effect of strain-rate upon the tensile deformation of materials, Journal of Engineering Materials and Technology, Vol. 97, Issue 2, 1975, pp. 151–155.

[33] Langseth B.M., Lindholm U.S., Larsen P.K., Lian B., Langseth M.U.S., Lindholm P. K., Larsen B.L., Strain rate sensitivity of mild steel grade St52-3N, Journal of Engeering

Mechanics, Vol. 117, 1991, pp. 719–732.

[34] Huh H., Kim S., Song J., Lim J., Dynamic tensile characteristics of TRIP-type and DP-type steel sheets for an auto-body, International Journal of Mechanical Sciences, Vol. 50, Issue 5, 2008, pp. 918–931.
DOI: 10.1016/j.ijmecsci.2007.09.004.

[35] Wellman B., Grain Size and Material Strength, Technical TIDBITS, No. 15, 2010, pp. 488–489.

[36] Zhang X.H., Lu X.B., Zhang L.M., Wang S.Y., Li Q.P., Experimental study on mechanical properties of methane-hydrate-bearing sediments, Acta Mechanica Sinica, Vol. 28, 2012, pp. 1356–1366.
DOI: 10.1007/s10409-012-0142-3.

[37] Hansen N., Hall-petch relation and boundary strengthening, Scripta Materialia, Vol. 51, Issue 8, 2004, pp. 801–806.
DOI: 10.1016/j.scriptamat.2004.06.002.

[38] Zhang X., Hansen N., Gao Y., Huang X., Hall-Petch and dislocation strengthening in graded nanostructured steel, Acta Materialia, Vol. 60, 2012, pp. 5933–5943.
DOI: 10.1016/j.actamat.2012.07.037.

[39] Couque H., Asaro R.J., Duffy J., Lee S.H., Correlations of microstructure with a dynamic and quasi-static fracture in plain carbon steel, Metallurgical Transactions A, Vol. 19, 1988, pp. 2179–2206.
DOI: 10.1007/BF02645043.